with the primer pairs described (*16*). CCR5 alone and with the forward construct (vMIP-I), the reverse construct (I-PIMv), and empty pMET7 vector were transfected into CCC/CD4 cells [A. McKnight, P. R. Clapham, R. A. Weiss, *Virology* **201**, 8 (1994)] by means of Lipofectamine (Gibco). After 48 hours, media was removed from the transfected cells and 1000 $TCID_{50}$ of SF162, M23, or ROD/B virus culture stock was added. Cells were washed four times after 4 hours of virus incubation and grown in DMEM with 5% FBS for 72 hours before immunostaining for HIV-1 p24 or HIV-2 gp105. Each condition was replicated three to four times with medians and error bars representing the standard deviations expressed as percentages of the foci formed in the presence of CCR5 alone.

29. G. Simmons *et al.*, *J. Virol.* **70**, 8355 (1996); P. R. Clapham, A. McKnight, R. A. Weiss, *J. Virol.* **66**, 3531 (1992).
30. P. M. Murphy, *Infect. Agents Dis.* **3**, 137 (1994); T. G. Senkevich *et al.*, *Science* **273**, 813 (1996); J.-C. Albrecht *et al.*, *J. Virol.* **66**, 5047 (1992); J. L. Gao and P. M. Murphy, *J. Biol. Chem.* **269**, 28539 (1994); M. S. Chee *et al.*, *Curr. Top. Microbiol. Immunol.* **154**, 125 (1990); R. F. Massung *et al.*, *Virology* **201**, 215 (1994).
31. R. Sarid, T. Sato, R. Bohenzky, J. Russo, Y. Chang, in preparation; E. Cesarman *et al.*, *J. Virol.* **70**, 8218 (1996); Y. Chang *et al.*, *Nature* **382**, 410 (1996); R. Sarid, P. S. Moore, Y. Chang, unpublished observation.
32. M. L. Cleary, S. D. Smith, J. Sklar, *Cell* **47**, 19 (1986); I. Palmero *et al.*, *Oncogene* **8**, 1049 (1993); C. Larcher *et al.*, *Eur. J. Immunol.* **25**, 1713 (1995); M. Birkenbach, K. Josefsen, R. Yalamanchili, G. Lenoir, E. Kieff, *J. Virol.* **67**, 2209 (1993).
33. G. Tosato, J. Tanner, K. D. Jones, M. Revel, S. E. Pike, *J. Virol.* **64**, 3033 (1990).
34. Y. Shen and T. E. Shenk, *Curr. Opin. Gen. Dev.* **5**, 105 (1995); K. H. Vousden, *Sem. Cancer Biol.* **6**, 109 (1995); L. J. Appleman and A. B. Frey, *Int. J. Cancer* **63**, 576 (1995).
35. A. Lichtenstein, Y. Tu, C. Fady, R. Vescio, J. Berenson, *Cell. Immunol.* **162**, 248 (1995).
36. C. Holzinger *et al.*, *Immunol. Lett.* **35**, 109 (1993).
37. A. Lafeuillade, G. Kaplanski, T. Allegre, J. P. de Jaureguiberry, *J. AIDS Hum. Retrovirol.* **12**, 95 (1996); T. Cohen, D. Nahari, L. W. Cerem, G. Neufeld, B.-Z. Levi, *J. Biol. Chem.* **271**, 736 (1996).
38. G. Scala *et al.*, *J. Exp. Med.* **172**, 61 (1990).
39. H. Harada *et al.*, *Science* **259**, 971 (1993).
40. A. M. Hardy, *J. AIDS* **4**, 386 (1991); G. F. Lemp, S. F. Payne, D. Neal, T. Temelso, G. W. Rutherford, *J. Am. Med. Assoc.* **263**, 402 (1990); R. Rothenberg *et al.*, *N. Engl. J. Med.* **317**, 1297 (1987); L. P. Jacobson *et al.*, *Am. J. Epidemiol.* **138**, 953 (1993); J. D. Lundgren, M. Melbye, C. Pederson, P. S. Rosenberg, J. Gerstoft, *ibid.* **141**, 652 (1995).
41. Abbreviations for the amino acid residues are: A, Ala; C, Cys; D, Asp; E, Glu; F, Phe; G, Gly; H, His; I, Ile; K, Lys; L, Leu; M, Met; N, Asn; P, Pro; Q, Gln; R, Arg; S, Ser; T, Thr; V, Val; W, Trp; and Y, Tyr.
42. The authors thank R. A. Bohenzky, J. Russo, and I. A. Edelman for collaborative work on genomic sequencing of KSHV; G. Simmons for help with HIV inhibition experiments, J. Strauchen for PEL tissue sections; Y.-Z. Cao, S. Silverstein, J. Luban and C. Parravicini for helpful discussions; R. Sarid, J. P. Parry, M. Yan, W. Zheng and A.-E. Thlick for technical assistance; and M. Davis and D. Holland for help in preparing the manuscript. Supported by NIH NCI grant CA67391, an award from the James S. McDonnell Foundation, the Cancer Research Campaign, and the Mercury Phoenix Trust.

30 August 1996; accepted 23 October 1996

A Role for Endothelial NO Synthase in LTP Revealed by Adenovirus-Mediated Inhibition and Rescue

David B. Kantor, Markus Lanzrein, S. Jennifer Stary, Gisela M. Sandoval, W. Bryan Smith, Brian M. Sullivan, Norman Davidson, Erin M. Schuman*

Pharmacological studies support the idea that nitric oxide (NO) serves as a retrograde messenger during long-term potentiation (LTP) in area CA1 of the hippocampus. Mice with a defective form of the gene for neuronal NO synthase (nNOS), however, exhibit normal LTP. The myristoyl protein endothelial NOS (eNOS) is present in the dendrites of CA1 neurons. Recombinant adenovirus vectors containing either a truncated eNOS (a putative dominant negative) or an eNOS fused to a transmembrane protein were used to demonstrate that membrane-targeted eNOS is required for LTP. The membrane localization of eNOS may optimally position the enzyme both to respond to Ca^{2+} influx and to release NO into the extracellular space during LTP induction.

Long-term potentiation, a form of synaptic plasticity, can be inhibited by agents that interfere with the activity of NO synthase (NOS), which suggests that NO serves as a retrograde messenger during some forms of LTP (*1*–*6*). Hippocampal slices from homozygous transgenic mice lacking neuronal NOS (nNOS), however, exhibited normal LTP (*7*). The LTP in slices from these mutant mice was still susceptible to inhibition by broad-spectrum NOS inhibitors, which suggests that another NOS isoform may participate in LTP. In fact, a residual NOS activity was detected in the hippocampus of these mice (*8*), perhaps resulting from endothelial NOS (eNOS) in CA1 neurons (*7*, *9*). Thus, eNOS may be the isoform of NOS that participates in LTP induction.

Division of Biology 216-76, California Institute of Technology, Pasadena, CA 91125, USA.

*To whom correspondence should be addressed. E-mail: schumane@cco.caltech.edu

Endothelial NOS is myristoylated and associated with membrane fractions (*10*–*12*). We assessed the subcellular localization of eNOS by examining the distribution of fluorescence in Chinese hamster ovary (CHO) cells transfected with a cDNA encoding a fusion protein composed of eNOS and green fluorescent protein (*13*, *14*) [the fluorescent protein used was Green Lantern (GL)] (*15*, *16*). Control cells transfected with GL alone exhibited a diffuse fluorescent signal throughout the cytoplasm and the nucleus (Fig. 1A), whereas the eNOS-GL fusion protein was localized in the plasmalemma membrane and intracellular membrane compartments (Fig. 1B) (*17*).

We examined the role of eNOS in LTP by combining pharmacological agents with recombinant adenovirus vectors that were designed to manipulate eNOS function. In control experiments, individual rat hippocampal slices were injected in the CA1 cell body region with an adenovirus vector containing *lac*Z (Ad-lacZ) (*15*, *18*). We examined synaptic transmission and plasticity at the Schaffer-collateral CA1 neuron synapses with conventional extracellular recording techniques (*19*). Control slices infected with Ad-lacZ exhibited staining for β-galactosidase (β-Gal) throughout the pyramidal cell layer and in processes extending into the stratum radiatum (SR) and stratum oriens (SO) within 4 to 8 hours of injection (Fig. 2A) (*18*); single pyramidal neurons expressing β-Gal were readily identified (Fig. 2B). Synaptic transmission (24 to 36 hours after infection) in Ad-lacZ–infected slices was indistinguishable from slices injected with control saline that were maintained for equivalent periods of time (Fig. 2C). In addition, short- and long-term synaptic plasticity, including post-tetanic potentiation (PTP), paired-pulse facilitation (PPF), and LTP, were normal (Fig. 2, C and D) [100-ms interstimulus interval (ISI) PPF, mean percent of the first field excitatory postsynaptic potential (fEPSP) slope ± SEM: saline, 126.2 ± 4.9% (n = 4); Ad-lacZ, 133.5 ± 4.5% (n = 4), not significant (NS); maximum PTP, mean percent of baseline ± SEM: saline, 345.0 ± 37.7% (n = 6); Ad-lacZ, 359.7 ± 21.9% (n = 6), NS; LTP, mean percent of baseline ± SEM: saline, 193.3 ± 25.3% (n = 6); Ad-lacZ, 184.7 ± 7.7% (n = 6), NS].

To address the role of eNOS in LTP, we constructed an adenovirus vector containing a truncated eNOS (Ad-TeNOS) (*15*). The truncated eNOS lacks catalytic activity yet retains the NH_2-terminal sequence required for myristoylation and may be a dominant negative inhibitor of eNOS function, presumably because it can heterodimerize with wild-type eNOS (*20*). Co-transfection of CHO cells with eNOS-GL

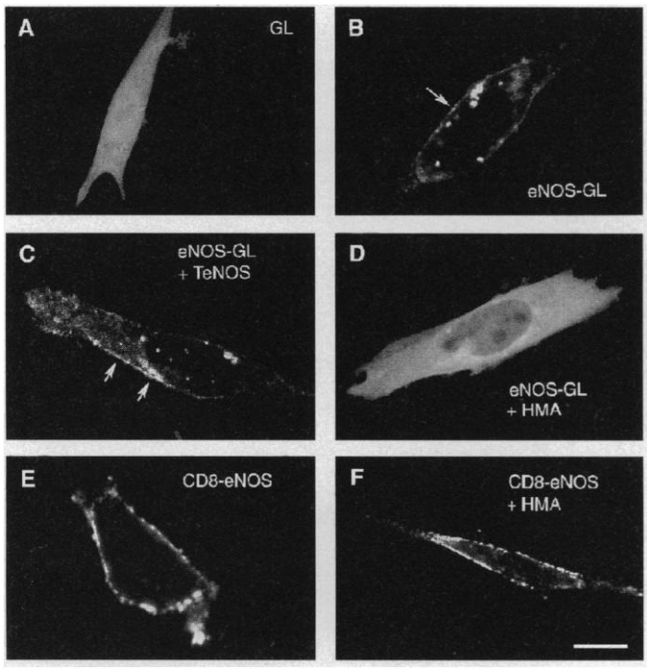

Fig. 1. Localization of endothelial NOS in transfected CHO cells. Confocal images of individual CHO cells transfected with the indicated constructs. (**A**) Cell transfected with a GL plasmid. (**B**) Cell transfected with an eNOS-GL fusion construct. (**C**) Cell cotransfected with eNOS-GL and TeNOS. (**D**) Cell transfected with eNOS-GL in the presence of the myristoylation inhibitor HMA. (**E**) CHO cell transfected with a plasmid containing a cDNA for a CD8-eNOS fusion protein immunofluorescently labeled with an antibody to CD8. (**F**) Cell transfected with CD8-eNOS in the presence of HMA. Scale bar, 5 μm.

and TeNOS (*16*) indicated that the coexpression of the truncation mutant did not significantly affect the subcellular localization of eNOS (Fig. 1C). The slight reduction in intensity of fluorescence associated with the plasma membrane (Fig. 1, B versus C) may be due to the fact that TeNOS–eNOS-GL heterodimers possess only a single fluorescent molecule, whereas eNOS-GL homodimers possess two copies.

Immunohistochemical studies of eNOS indicate that eNOS is preferentially associated with the apical dendrites of CA1 neurons in SR but appears to be absent from the basal dendrites in SO (*7*, *9*). As is consistent with this localization, LTP is blocked by NOS inhibitors at the apical, but not the basal, synapses of CA1 neurons (*21*). We conducted a blind study (*19*) in which LTP was simultaneously examined at both SR and SO synapses in slices infected 24 to 36 hours earlier with either Ad-lacZ or Ad-TeNOS. Control slices infected with Ad-lacZ displayed normal LTP at both SR and SO synapses (Fig. 3, A and B) [mean percent of baseline: SR, 213.9 ± 12.8% (n = 19); SO, 225.3 ± 30.3 (n = 11)] (*22*). In contrast, slices infected with Ad-TeNOS virus exhibited robust LTP at SO synapses but failed to exhibit LTP at SR synapses (Fig. 3, C and D) [mean percent of baseline: SO, 250.4 ± 26.4% (n = 11); SR: 108.9 ± 4.8 (n = 20)]. Ad-TeNOS–infected slices displayed normal synaptic transmission, PPF, and PTP as compared with Ad-lacZ control slices [input-output slope mean ± SEM: Ad-lacZ, 0.011 ± 0.002 (n = 6); Ad-TeNOS, 0.009 ± 0.003 (n = 6), NS; 100-ms ISI PPF, mean percent of first fEPSP slope ± SEM: Ad-lacZ, 136.1 ± 6.4% (n = 4), Ad-TeNOS, 146.0 ± 18.0% (n = 4), NS; maximum PTP, mean percent of baseline ± SEM: Ad-lacZ, 330.2 ± 21.2% (n = 19); Ad-TeNOS, 351.0 ± 32.7% (n = 20), NS]. Taken together, the lack of effect on basal synaptic strength and short-term plasticity as well as the selective inhibition of LTP in SR suggest that Ad-TeNOS abolishes potentiation by interfering with eNOS function in the apical dendrites of CA1 pyramidal neurons.

The fatty acid myristate is cotranslationally added to the NH_2-terminal glycine of eNOS (*10*–*12*) but not of nNOS. Myristoylation is accomplished by an *N*-myristoyltransferase (NMT) activity, which is extremely abundant in the hippocampus (*23*). We determined the effect of a myristoylation inhibitor, hydroxymyristic acid (HMA) (*24*, *25*), on the distribution of

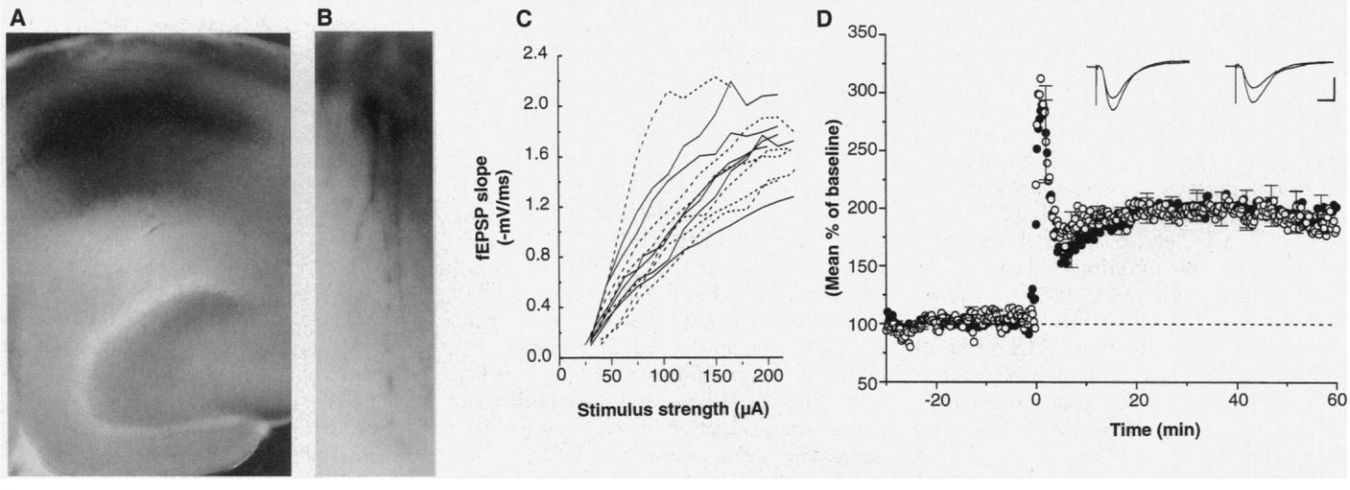

Fig. 2. Hippocampal slices infected with an Ad-lacZ construct exhibit normal synaptic transmission and plasticity. (**A**) An Ad-lacZ slice infected in area CA1 stained for X-Gal 24 hours after injection. (**B**) β-Gal labeling of individual pyramidal neurons and their associated dendrites. Scale bar in (A), 150 μm; in (B), 15 μm. (**C**) I/O relation for control (saline-injected) slices (solid lines) and slices infected with Ad-lacZ (dashed lines). The slope of each line was calculated, and a between-group comparison indicated that they are not significantly different from one another [mean slope ± SEM: Ad-lacZ, 0.011 ± 0.002; saline, 0.01 ±0.001 (NS)]. (**D**) Ensemble average of LTP experiments for both control and Ad-lacZ slices. In control slices (filled circles), the mean field EPSP slope before LTP was −0.14 ± 0.01 mV/ms (mean ± SEM) and −0.27 ± 0.05 mV/ms after LTP (P < 0.01). In Ad-lacZ slices (open circles), the mean field EPSP slope before LTP was −0.16 ± 0.01 mV/ms (mean ± SEM) and −0.28 ± 0.03 mV/ms after LTP (P < 0.01). Two representative field EPSPs, taken 10 min before and 50 to 60 min after LTP are shown. Traces on the right are from an Ad-lacZ slice; traces on the left are from a control slice. Calibration bar: 0.5 mV, 10 ms.

eNOS-GL in CHO cells. Treatment with HMA abolished the membrane localization of eNOS and resulted in a diffuse localization of eNOS throughout the cytoplasm (Fig. 1D), yielding a fluorescence pattern similar to that observed for GL alone (Fig. 1A). These data confirm that myristoylation is required for the membrane localization of eNOS (*12*, *26*).

We next examined whether the NMT inhibitor could attenuate LTP. We treated slices with HMA for 20 to 26 hours before electrophysiological recordings (*27*) in order to interfere with the myristoylation of newly synthesized eNOS (*28*). Hippocampal slices incubated in HMA failed to exhibit LTP, whereas control slices exhibited significant potentiation (Fig. 4A) [mean percent of baseline: HMA, 112.4 ± 4.0% (n = 14); control, 187.2 ± 13.8% (n = 13); $P <$ 0.001]. The HMA-treated slices (which failed to exhibit LTP) showed significantly reduced NMT activity when compared to control slices (*29*) [NMT activity in adjusted CPM: HMA, 363.4 ± 36.6 (n = 9); control, 3788.5 ± 531.6 (n = 8); $P < 0.001$]. Short-term extracellular application of HMA to slices (50 min before LTP induction) did not affect LTP (Fig. 4B), which suggests that the inhibitory effects of long-term HMA treatment were due to the prevention of myristoylation rather than to a nonspecific synaptic effect (for example, antagonizing NMDA receptors or protein kinase activity).

To rule out the possibility that a myristoyl protein other than eNOS is required for LTP and to directly assess whether eNOS is the critical myristoyl protein affected by inhibition of myristoylation, we designed a chimeric protein. The chimera contained the extracellular and transmembrane domain of CD8 (*30*) fused to an eNOS lacking the NH_2-terminal glycine required for myristoylation (*12*), thus providing an alternate means of membrane association (*15*). We verified the catalytic NOS activity of the CD8-eNOS fusion protein in transfected CHO cells (*20*). Like eNOS-GL, CD8-eNOS was localized in the plasma membrane in transfected CHO cells (Fig. 1E). Incubation of CD8-eNOS–transfected CHO cells with HMA did not alter the membrane localization of CD8-eNOS fluorescence (Fig. 1F), verifying that the CD8-fusion protein can confer membrane localization via a myristoylation-independent pathway.

We then tested whether slices infected with the CD8-eNOS construct could be rescued from the HMA-induced inhibition of LTP. In blind experiments, slices injected with Ad-lacZ and incubated with HMA still failed to exhibit LTP, whereas slices injected with Ad–CD8-eNOS and incubated with HMA exhibited fully restored and robust potentiation (Fig. 4C) [mean percent of baseline: Ad-lacZ + HMA, 108.2 ± 8.4% (n = 8); Ad–CD8-eNOS + HMA, 185.6 ± 20.9% (n = 9); $P < 0.01$]. Both groups of slices exhibited similar PPF and input-output (I/O) relations for synaptic responses to stimuli of varying strengths [PPF mean percent of the first EPSP slope: Ad-lacZ + HMA, 137.1 ± 6.2% (n = 6); Ad–CD8-eNOS + HMA, 126.2 ± 2.2% (n = 8), NS; I/O slope mean ± SEM: Ad-lacZ + HMA, 0.011 ± 0.002 (n = 7); Ad–CD8-eNOS + HMA: 0.010 ± 0.001 (n = 8), NS]. The Ad–CD8-eNOS rescue was prevented when HMA-treated slices were also incubated in a NOS inhibitor, which indicates that the restoration of LTP requires NOS activity (Fig. 4C) [mean percent of baseline: Ad–CD8-eNOS + HMA + NOS inhibitor, 106.8 ± 3.4% (n = 6), NS]. These results establish that membrane localization of eNOS via a transmembrane domain can restore LTP in myristoylation-inhibited slices and suggest that, under these experimental conditions, eNOS is the only myristoyl protein that is required for LTP production. As HMA selectively perturbs the localization of eNOS without diminishing the apparent amount of eNOS (Fig. 1D), these data suggest that membrane-associated, rather than cytosolically localized, eNOS is critical for LTP.

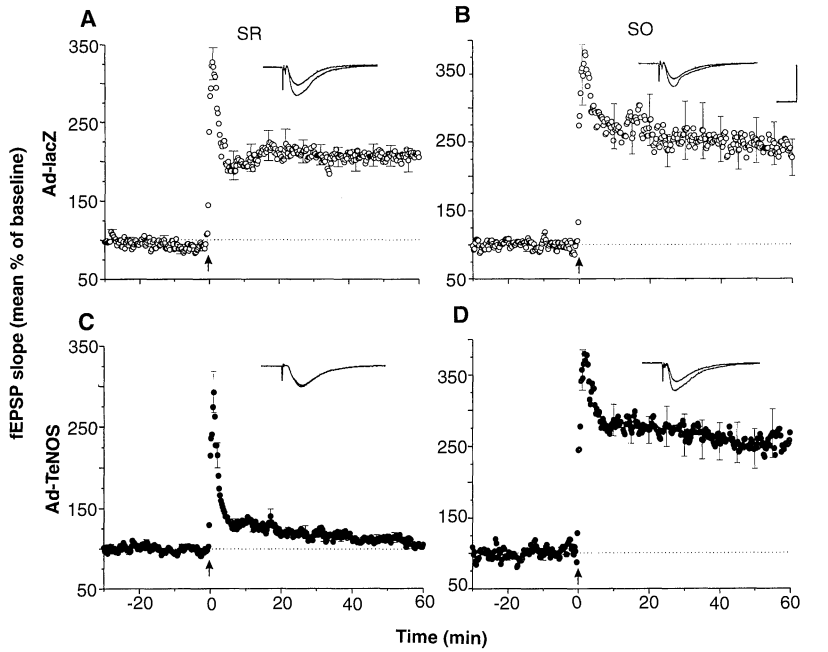

Fig. 3. Infection of CA1 neurons with TeNOS blocks LTP at SR but not SO synapses. (**A** through **D**) Two superimposed representative field EPSPs, taken 10 min before and 50 to 60 min after LTP. In Ad-lacZ slices, LTP was exhibited at both SR (A) and SO (B) synapses. The mean fEPSP slope in SR before LTP was −0.17 ± 0.04 mV/ms (mean ± SEM) and −0.29 ± 0.03 mV/ms after LTP ($P < 0.01$). The mean fEPSP slope in SO before LTP was −0.17 ± 0.02 mV/ms (mean ± SEM) and −0.39 ± 0.07 mV/ms after LTP ($P < 0.01$). In Ad-TeNOS slices, LTP was attenuated at SR synapses (C), but not SO synapses (D). The mean fEPSP slope in SR before LTP was −0.14 ± 0.04 mV/ms (mean ± SEM) and −0.15 ± 0.06 mV/ms after LTP ($P \leq 0.05$). The mean fEPSP slope in SO before LTP was −0.20 ± 0.05 mV/ms (mean ± SEM) and −0.48 ± 0.19 mV/ms after LTP ($P \leq 0.01$). Calibration bar: 1.0 mV, 10 ms.

A previous study (*7*) in $nNOS^{-/-}$ mice suggested that eNOS may participate in LTP, although its role as either the primary NOS isoform or as a compensatory isoform was unclear. Our data indicate that eNOS, rather than nNOS, is the primary NOS isoform used in LTP and that no compensation by nNOS can occur when eNOS membrane localization is acutely perturbed in the adult animal. Because eNOS is the only NOS family member that is a myristoyl protein, the block of LTP by HMA and the subsequent rescue with the CD8-eNOS fusion protein indicates a lack of compensation by nNOS in the adult animal.

Previous studies (*2*, *3*) with NOS inhibitors injected into individual CA1 neurons suggested a postsynaptic requirement for NOS activity. In addition, eNOS is localized to the dendrites (*7*, *9*) or synaptic fractions (*31*) of CA1 neurons. Thus, it is likely that observed effects of eNOS manipulation in this study are due to actions in postsynaptic CA1 neurons, although alternative sites, such as glia, cannot be ruled out. In COS-7 cells, the myristoylation of eNOS and its consequent membrane localization facilitate the extracellular release of NO (*17*, *32*), raising the possibility that membrane localization of eNOS is neces-

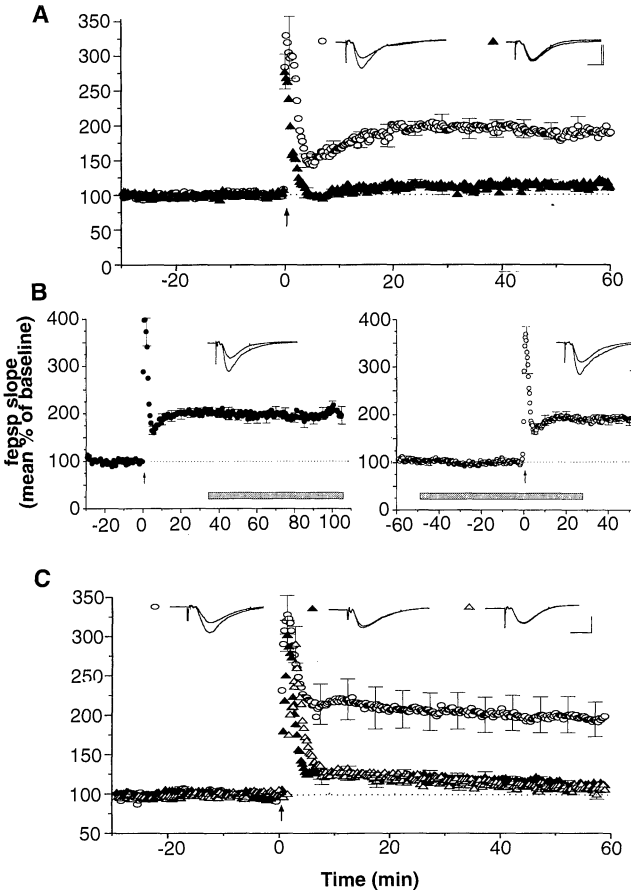

Fig. 4. Membrane targeting of eNOS with an Ad–CD8-eNOS fusion protein rescues the block of LTP by myristoylation inhibition. (**A** through **C**) Two superimposed representative fEPSPs, taken 10 min before and 50 to 60 min after LTP. (A) Slices incubated with HMA for 20 to 26 hours do not exhibit LTP. The ensemble average of LTP experiments for both control (open circle) and HMA-treated (closed triangle) slices is shown. In control slices, the mean fEPSP slope before LTP was −0.17 ± 0.01 mV/ms (mean ± SEM) and −0.32 ± 0.03 mV/ms after LTP ($P < 0.001$). In HMA-treated slices, the mean fEPSP slope before LTP was −0.18 ± 0.01 mV/ms (mean ± SEM) and −0.21 ± 0.02 mV/ms after LTP ($P < 0.05$). (B) Acute extracellular application of HMA does not affect LTP induction or maintenance. Shown are ensemble averages of two-pathway experiments. HMA (100 μM) was applied at the times indicated by bars. (Right) The mean fEPSP slope before LTP was −0.10 ± 0.01 mV/ms (mean ± SEM) and −0.20 ± 0.02 mV/ms after LTP ($P < 0.001$). (Left) The mean fEPSP slope before LTP was −0.13 ± 0.01 mV/ms (mean ± SEM) and −0.22 ± 0.04 mV/ms after LTP ($P < 0.05$). (C) Slices infected with a CD8-eNOS adenovirus construct can be rescued from inhibition by a myristoylation inhibitor. Shown are ensemble averages for HMA-treated slices infected with Ad-lacZ (closed triangle), Ad–CD8-eNOS (open circle), or Ad–CD8-eNOS + a NOS inhibitor (open triangle). In Ad-lacZ HMA-treated slices, the mean fEPSP slope before LTP was −0.12 ± 0.00 mV/ms (mean ± SEM) and −0.13 ± 0.01 mV/ms (NS) after LTP. In CD8-eNOS HMA-treated slices, the mean fEPSP slope before LTP was −0.13 ± 0.01 mV/ms (mean ± SEM) and −0.25 ± 0.03 mV/ms after LTP ($P < 0.01$). In CD8-eNOS HMA and NOS inhibitor–treated slices, the mean fEPSP slope before LTP was −0.12 ± 0.01 mV/ms (mean ± SEM) and −0.12 ± 0.01 mV/ms after LTP (NS).

sary for NO to fulfill its proposed role of a retrograde messenger. Indeed, the association of eNOS with the plasma membrane might position the enzyme in an ideal location both to respond to Ca^{2+} influx and to release NO into the extrasynaptic region during LTP induction.

REFERENCES AND NOTES

1. G. A. Böhme, C. Bon, J.-M. Stutzmann, A. Doble, J.-C. Blanchard, *Eur. J. Pharmacol.* **199**, 379 (1991).
2. E. M. Schuman and D. V. Madison, *Science* **254**, 1503 (1991).
3. T. J. O'Dell, R. J. Hawkins, E. R. Kandel, O. Arancio, *Proc. Natl. Acad. Sci. U.S.A.* **88**, 11285 (1991).
4. J. E. Haley, G. L. Wilcox, P. F. Chapman, *Neuron* **8**, 211 (1992).
5. E. M. Schuman and D. V. Madison, *Science* **263**, 532 (1994).
6. However, several groups [D. M. Chetkovich, E. Klann, J. D. Sweatt, *NeuroReport* **4**, 919 (1993); V. K. Gribkoff and J. T. Lum-Ragan, *J. Neurophysiol.* **68**, 639 (1992); J. E. Haley, P. L. Malen, P. F. Chapman, *Neurosci. Lett.* **160**, 85 (1993); J. H. Williams *et al.*, *Neuron* **11**, 877 (1993); J. A. Cummings, S. M. Nicola, R. C. Malenka, *Neurosci. Lett.* **176**, 110 (1994)] have shown that NO-independent forms of LTP can be elicited with different stimulation protocols.
7. T. J. O'Dell *et al.*, *Science* **265**, 542 (1994).
8. P. L. Huang, T. M. Dawson, D. S. Bredt, S. H. Snyder, M. C. Fishman, *Cell* **75**, 1273 (1993).
9. J. L. Dinerman, T. M. Dawson, M. J. Schell, A. Snowman, S. H. Snyder, *Proc. Natl. Acad. Sci. U.S.A.* **91**, 4214 (1994).
10. J. Pollock, V. Klinghofer, U. Forstermann, F. Murad, *FEBS Lett.* **309**, 402 (1992).
11. J. Liu and W. C. Sessa, *J. Biol. Chem.* **269**, 11691 (1994).
12. L. Busconi and T. Michel, *ibid.* **268**, 8410 (1993).
13. R. Helm, A. B. Cubitt, R. Y. Tsien, *Nature* **373**, 663 (1995).
14. M. Chalfie, Y. Tu, G. Euskirchen, W. W. Ward, D. C. Prasher, *Science* **263**, 802 (1994).
15. The cDNA constructs and adenovirus vectors were made as follows. For eNOS-GL, an in-frame Xba I site was generated by polymerase chain reaction (PCR) 3′ to the coding region of eNOS (in pAC) and 5′ to the coding region of GL (in pCDNA3). The two coding regions were then joined at the Xba I site by being subcloned into the pAC cytomegalovirus (CMV) adeno transfer vector [A. M. Gomez-Foix *et al.*, *J. Biol. Chem.* **267**, 25129 (1992)]. For TeNOS, the eNOS cDNA in pBluescript SK was digested with Kpn I, yielding a fragment encoding the first 737 NH_2-terminal amino acids that was subcloned in the Kpn I site of pAC CMV. Insertion into the Kpn I site generated an in-frame stop codon beginning at base pair 25 of the pUC 19 polylinker, which was confirmed by DNA sequencing. For CD8-eNOS, a cDNA encoding the extracellular, transmembrane, and seven amino acids of the intracellular domain of CD8 [V. P. Sukhatme *et al.*, *Cell* **40**, 591 (1985)] was isolated by PCR from the vector with primers that created a 5′ Eco RI and a 3′ Cla I site. eNOS cDNA with a mutation in the *N*-myristoylation consensus sequence [Gly^2 to Ala^2 (G2A)] in pBluescript SK was excised at the 5′ Cla I site and the 3′ Xba I site. In a three-way ligation, the CD8 and eNOSG2A fragments were subcloned into pBluescript SK. Orientation was confirmed by restriction analysis, and the junction sequence of the CD8-eNOS G2A fusion was confirmed by DNA sequencing. The fusion cDNA was then excised with Eco RI, subcloned into pAC CMV, and screened for orientation. Membrane localization was confirmed by immunocytochemistry with a fluorescein-conjugated monoclonal antibody to human CD8 (Sigma). Recombinant adenoviruses were prepared by standard transfection methods into HEK 293 cells, with the use of the experimental plasmids plus the right arm of the Ad5pAC I virus digested with Xba I and Cla I. This virus contains a 2.7-kb deletion in the E3 region, thus providing adequate cloning capacity for all inserts.
16. CHO cells were maintained and propagated under standard conditions (5% CO_2 in Ham's F12 medium containing 10% fetal bovine serum). One day before the transfection, the cells were seeded into 30-mm dishes at 2 × 10^5 cells per dish. A thin glass cover slip was embedded in the bottom of the plastic dish to enable the use of oil immersion lenses in confocal microscopy. CHO cells were transfected with pGreenlantern-1 (Gibco-BRL, Gaithersburg, MD), pACeNOS-GL, or pACCD8-eNOS (2 μg of plasmid DNA per dish), or were cotransfected with pACeNOS-GL and pACTeNOS at a ratio of 1:3 (8 μg of plasmid DNA per dish). When added, HMA was at a final concentration of 100 μM and ethanol was at a final concentration of 0.25%. Transfections were carried out with lipofectamine (Gibco-BRL) according to the manufacturer's instructions. After transfection (20 to 24 hours), the cells were analyzed with an inverted-stage laser confocal microscope system (BioRad MRC-600) using an argon laser, an excitation wavelength of 488 nm, and a ×63 objective. Contrast and brightness settings were constant between experiments. Images were imported and displayed in Adobe Photoshop 3.0.
17. W. C. Sessa *et al.*, *J. Biol. Chem.* **270**, 17641 (1995).
18. Hippocampal slices were infected by microinjection of viral stock into the extracellular space of the CA1 pyramidal cell layer with glass micropipettes with tips broken off (resistance <1 megaohm). Injections were made along the area of CA1 corresponding to the full extent of the inner blade of the dentate gyrus. For each injection position in CA1, multiple pressure injections of short duration (three injections per site of 10 to 20 sites per slice for 100 ms at 5 to 10 psi) were made by advancing the electrode through the depth of the slice. After injections, slices were maintained in 250 μl of minimum essential medium (MEM) as described below for 4 to 30 hours (mean ± SEM: 27.1 ± 0.4 hours), after which field potential recordings were conducted in normal Ringer's solution. Slices were maintained at 22°C to 25°C in a MEM consisting of Kreb Ringer's solution (119 mM NaCl, 2.5 mM KCl, 1.3 mM $MgSO_4$, 2.5 mM $CaCl_2$, 2.5 mM NaH_2PO_4, and 26.2 mM $NaHCO_3$) supplemented with B-27, 20 mM glucose, 250 μM glutamine, and penicillin-streptomycin (50 U/ml). Individual slices were placed in 24-well plates with 250 μl of solution in a humidified 95% O_2/5% CO_2 atmosphere. One-half of the volume of the medium was ex-

changed every 12 hours. β-Gal was detected with X-Gal staining [J. R. Sanes, J. L. R. Rubenstein, J.-F. Nicolas, *EMBO J.* **5**, 3133 (1986)]. In 50-μm sections of infected slices, we counted the number of neurons containing β-Gal, and estimated that 68 to 95% of neurons in the injected region were infected, depending on whether central or peripheral regions of virus injection were scrutinized. Stained slices were photographed (Zeiss Axiophot, ×2.5 and ×10 objectives) and imported into Adobe Photoshop 3.0 for graphic presentation.

19. Hippocampal slices (500 μm) were prepared from young adult male Sprague-Dawley rats. Slices were submerged in a stream of artificial cerebral spinal fluid (ACSF) (119 mM NaCl, 2.5 mM KCl, 1.3 mM $MgSO_4$, 2.5 mM $CaCl_2$, 1.0 mM Na_2HPO_4, 26.2 mM NaH_3CO, and 11.0 mM glucose), maintained at 22°C to 25°C, and gassed with 95% O_2/5% CO_2. fEPSPs measured independently in SR or SO at a depth of 100 to 150 μm below the slice surface were evoked by two different stimulating electrodes activating the Schaffer collateral-commissural afferents (once every 15 s); the initial (1- to 2-ms) slope was measured. LTP was induced by four trains of high-frequency stimulation (100 Hz for 1 s) separated by 30-s intervals. To quantify I/O relations, the slopes of the regression lines for each experiment were compared. All electrophysiology experiments, with the exception of those noted in (*22*), were conducted with the experimenter being unaware of the experimental condition of the slice. The percents of baseline measurements indicated in the text were taken 50 to 60 min after tetanus. Ensemble average plots represent group means of each EPSP slope, for all experiments, aligned with respect to the time of LTP induction. To assess statistical significance, paired or independent *t* tests were performed. *P* values greater than 0.05 are designated as NS.
20. C. M. Lee, L. J. Robinson, T. Michel, *J. Biol. Chem.* **270**, 27403 (1995). We examined whether the expression of TeNOS inhibits NOS catalytic activity by monitoring the Ca^{2+}-dependent conversion of [^{14}C]arginine to [^{14}C]citrulline in hippocampal homogenates made from infected CA1 regions of hippocampal slices [D. S. Bredt and S. H. Snyder, *Proc. Natl. Acad. Sci. U.S.A.* **86**, 9030 (1989)]. (The NOS activity of Ad–CD8-eNOS was assessed in CHO cells with the same method.) We found that Ad-TeNOS inhibited NOS activity by 14.4 ± 3.2% when compared with Ad-lacZ–infected slices (n = 6 experiments, 3 slices per experiment, for both Ad-lacZ and Ad-TeNOS). This modest but significant inhibition may reflect the relatively small contribution of eNOS to the total NOS activity detected in the hippocampus (*7*) and may account for the observed block of LTP in SR by TeNOS, although alternative mechanisms may also contribute.
21. J. E. Haley and D. V. Madison, *Learn. Mem.*, in press.
22. We combined the simultaneous SR-SO experiments shown in Fig. 3 with an earlier blind study examining LTP in Ad-lacZ– versus TeNOS-infected slices at SR synapses only, because the two sets of SR data were statistically indistinguishable from one another.
23. R. A. J. McIlhinney and K. MGlone, *J. Neurochem.* **54**, 110 (1990).
24. M. J. S. Nadler, M. L. Harrison, C. L. Ashendel, J. M. Cassady, R. L. Geahlen, *Biochemistry* **32**, 9250 (1993).
25. L. A. Paige, G. Zheng, S. A. De Frees, J. M. Cassady, R. L. Geahlen, *ibid.* **29**, 10566 (1990).
26. L. Busconi and T. Michel, *J. Biol. Chem.* **269**, 25016 (1994).
27. Slices were treated with 100 μM HMA dissolved in ethyl alcohol (EtOH) and bovine serum albumin (BSA) (final EtOH concentration, 0.25%; final BSA concentration, 0.25 mg/ml) or with vehicle alone and were maintained in the same MEM described above for 20 to 26 hours before electrophysiological recording. Adjacent slices from one hippocampus were exposed to either experimental or control conditions, and only data from pairs in which the control slice expressed LTP were considered. For experiments in which HMA was applied acutely, a two-pathway design was implemented. HMA dissolved in EtOH plus BSA was added directly to the superfusate at the indicated times, and during the control recording period, slices were perfused with Ringer's containing EtOH plus BSA. In experiments using a NOS inhibitor, L-*N*-monomethyl-arginine (100 μM; Sigma) was applied to slices for at least 3 hours before recording.
28. The half-life of eNOS has been reported to be approximately 20 hours [L. J. Robinson, L. Busconi, T. Michel, *J. Biol. Chem.* **270**, 995 (1995); D. J. Stuehr and O. W. Griffith, *Adv. Enzymol. Relat. Areas Mol. Biol.* **65**, 287 (1992)].
29. NMT activities in homogenates made from the same slices used for electrophysiology were determined as described [M. J. King and R. K. Sharma, *Anal. Biochem.* **199**, 149 (1991)] with a post-hoc assay that measures the transfer of [^{3}H]myristic acid to a synthetic acceptor peptide—the eight NH_2-terminal amino acids of pp60^{src}. [^{3}H]myristoyl coenzyme A was generated enzymatically [D. Towler and L. Glaser, *Proc. Natl. Acad. Sci. U.S.A.* **83**, 2812 (1986)], and the NMT activity assay was performed on 50 μg of homogenate protein. Data are expressed as adjusted counts per minute (cpm).
30. P. Sukhatme, K. C. Sizer, A. C. Vollmer, T. Hunkapiller, J. R. Parnes, *Cell* **40**, 591 (1985).
31. D. B. Kantor and E. M. Schuman, unpublished observations.
32. T. Sakoda *et al.*, *Mol. Cell. Biochem.* **152**, 143 (1995).
33. We thank T. Michel for sharing various eNOS cDNAs and unpublished results, B. Seed for CD8 cDNA, A. Berk and L. Wu for Ad-lacZ, and G. Laurent for technical assistance and discussion. Supported by European Molecular Biology Organization grant ALTF 168-1996 (M.L.), National Institute of Mental Health grant 49176 (N.D.), NIH grant NS37292 (E.M.S.), and a Beckman Young Investigator award (E.M.S.).

27 August 1996; accepted 23 October 1996

TECHNICAL COMMENTS

Mechanisms of Punctuated Evolution

In their report, "Punctuated evolution caused by selection of rare beneficial mutations," Santiago F. Elena *et al.* describe (*1*) punctuated changes in a morphological character (cell size) in a population of *Escherichia coli* kept in batch culture with daily transfer for 3000 generations. They state that their observations might explain some aspects of punctuated evolutionary change, a phenomenon often said to be inconsistent with classical neo-Darwinism (*2*). The controversy about punctuated equilibrium involves two questions: (i) How ubiquitous is the pattern of "jerky" evolution in nature? and (ii) Do novel evolutionary processes cause this pattern? Elena *et al.* answer the second question by proposing that stasis in the fossil record arises (as it does in their bacteria) from an absence of genetic variation, while rapid changes in the record reflect the spread of new beneficial mutations.

Although the report (*1*) by Elena *et al.* provides useful evidence of the power of selection to produce rapid evolutionary change, there are substantial problems in relating the results to the fossil record. First, their experiment was designed so that punctuated change was the only conceivable outcome. Second, the phenomenon of punctuation in such laboratory populations is not novel, but has been described many times in the literature. Third, it is unwarranted to extrapolate evolution in a clonal population of *E. coli* to punctuated evolution in sexual eukaryotes.

By beginning their experiment with a genetically uniform clonal population, Elena *et al.* virtually guaranteed a punctuated outcome. Because there was no initial genetic variation, all evolutionary change was constrained to occur by the successive fixation of newly arising mutations (*3*). Many related experiments in flies and mice have shown that, in small or highly inbred populations, the response to artificial selection stops when genetic variation is exhausted, but can undergo sudden jumps on the appearance of new mutations of large effect (*4*). Indeed, periodic selection in bacteria, a phenomenon described by Atwood and his colleagues (*5*), is simply the sporadic occurrence of mutations with a large effect on fitness.

The relevance of observations on clonal or inbred populations to the fossil record is highly questionable; patterns of punctuated evolution in nature can be explained without appealing to the episodic fixation of new mutations. Most fossils come from sexually reproducing populations that are large enough to leave an adequate record (*6*). In such populations, rapid (on a geological scale) evolution in response to environmental changes can be caused by selection acting on genetically variable traits (*7*). There are many well-documented examples of rapid, episodic change in contemporary natural populations (*8*), and artificial selection in large laboratory populations has produced rates of change of orders of magnitude faster than those seen in the fossil record (*9*). Once the environment has stopped changing drastically, stabilizing selection will act to preserve the optimum phenotype, and morphological change will slow down or cease, producing the appearance of stasis. Given the unpredictable nature of environmental change, it is thus not unexpected that evolution often goes in fits and starts, a fact that has long been recognized (*6*, *10*).